Eur. Phys. J. A **25**, 199–209 (2005)
DOI 10.1140/epja/i2005-10080-8

THE EUROPEAN PHYSICAL JOURNAL A

Giant dipole resonance and shape transitions in warm and rapidly rotating nuclei

P. Arumugam[1,a], A. Ganga Deb[2], and S.K. Patra[1]

[1] Institute of Physics, Sachivalaya Marg, Bhubaneswar - 751 005, India
[2] Department of Physics, Sonepur College, Subarnapur - 767017, Orissa, India

Received: 28 April 2005 /
Published online: 26 August 2005 –
Communicated by Th. Walcher

Abstract. We discuss the shape transitions in few medium heavy-mass nuclei with emphasis on low-temperature behaviour of the giant dipole resonance (GDR) observables. We employ a macroscopic approach towards GDR in which the GDR observables are related to the nuclear shapes. Shape calculations were done using the cranked Nilsson-Strutinsky method (CNSM) extended to finite temperature. Thermal shape fluctuations are computed with free energies calculated employing Landau parameterization as well as those calculated exactly (without using parameterizations) at given spin and temperature. The results obtained are confronted with the experimental data wherever available. Our study reveals that if the fluctuations are treated properly, then, in spite of thermal fluctuations, GDR observables could very well reflect the shape transitions at low temperature.

PACS. 24.30.Cz Giant resonances – 21.60.-n Nuclear structure models and methods – 24.60.-k Statistical theory and fluctuations

1 Introduction

Isovector giant dipole resonance commonly termed as GDR is one among the fundamental modes of excitations in nuclei caused by the photons [1]. In a microscopic picture, GDR can be understood in terms of particle-hole excitations often called p-h doorway resonance [2,3]. Alternatively, macroscopic approaches couple the GDR to the shape of the nuclei [4–7]. The GDR spectrum could effectively reflect the structure of the nuclear state on which GDR is built. For hot rotating nuclei, GDR serves as a unique probe to obtain the structure information. Hence GDR studies of nuclei as a function of both temperature (T) and spin (I) have been an interesting and important area of research in nuclear-structure physics. Recent developments on the theoretical [7–9] and experimental [10–13] fronts could shed more light in our understanding of hot rotating nuclei. However, several key issues remain to be understood [14]. One among them is the variation of the GDR width ($\Gamma_{\rm GDR}$) as a function of T and I.

In the ground state, the GDR observables, primarily the $\Gamma_{\rm GDR}$ can be directly related to the equilibrium deformation (β). For hot and rotating nuclei the $\Gamma_{\rm GDR}$ is influenced significantly by three factors *viz*, 1) change in β, 2) due to thermal shape fluctuations the averaged deformation ($\bar{\beta}$) may increase which leads to the increase of $\Gamma_{\rm GDR}$ with increasing T and 3) Coriolis splitting of GDR components may increase $\Gamma_{\rm GDR}$, which happens at higher spins. Among the above factors, the thermal fluctuations are observed to be more dominant. Hence, as the temperature increases, generally $\Gamma_{\rm GDR}$ increases irrespective of the trend of β (which in most of the cases would be decreasing). In observations at fixed T and varying I, $\Gamma_{\rm GDR}$ was found to follow the trend of β and $\bar{\beta}$. In this case we observe that the gross structure effects do survive thermal fluctuations and changes in the equilibrium shape could be probed by the GDR [15]. However, in any case, there is a direct correlation between $\bar{\beta}$ and $\Gamma_{\rm GDR}$ and few explicit relations are derived [9,16].

At low temperatures when fluctuations are not very dominant, the averaged shape ($\bar{\beta}$) could well reflect the changes in the equilibrium shape (β). Hence, it would be interesting to carry out investigations in such cases where better and clear correlations between $\Gamma_{\rm GDR}$ and β do exist. With recent experimental techniques, few low-T measurements have been made [10,11] and the data could not be explained by conventional thermal-fluctuation calculations. At low T, microscopic effects such as shell and pairing effects could make important contributions [7,8].

[a] *Present address*: Centro de Física das Interacções Fundamentais, Instituto Superior Tecnico, Avenida Rovisco Pais, P1049-001 Lisbon, Portugal; e-mail: aru@iopb.res.in

Hence, care should be taken while applying the theories which were successful in the high-T regime. One among the major concerns in this regard is the applicability of free-energy parameterizations such as Landau theory [5, 17] which were employed to do time-saving calculations. In a previous work [7], some of us have presented a simple theoretical framework for calculating GDR observables without employing the free-energy parameterizations. In ref. [18] few discrepancies in applying the free-energy parameterizations at low T and high spins were pointed out and they were ascribed to spin-dependent shell corrections which the existing parameterizations do not account for. In the present work, we study in detail the shape transitions in few selected medium heavy-mass nuclei with an emphasis on the low-T behaviour of these nuclei and its consequences on GDR observables.

In the next section, we present our theoretical framework in an illustrative way comprising the details about temperature dependence of shell corrections. In sect. 3, we discuss our results for few selected medium heavy-mass nuclei along with the experimental data wherever available. The conclusions are drawn in sect. 4.

2 The formalism

Some details of our theoretical formalism for studying giant dipole resonance can be found in refs. [7,18]. Here we present the cranked Nilsson-Strutinsky method (CNSM) in an illustrative way and outline the other parts. The formalism can be explained in three folds with models for 1) shape calculations, 2) relating the shapes to GDR observables and 3) considering the shape fluctuations due to thermal effects. The important details of these three parts are presented in the following subsections.

2.1 Cranked Nilsson-Strutinsky method at finite temperature

In this approach [7,18], the total free energy ($F_{\rm TOT}$) at fixed deformation is calculated using the expression

$$F_{\rm TOT} = E_{\rm RLDM} + \sum_{p,n} \delta F \, . \tag{1}$$

Expanding the rotating liquid-drop model (LDM) energy $E_{\rm RLDM}$ and writing shell corrections in the rotating frame [19] leads to

$$F_{\rm TOT} = E_{\rm LDM} + \sum_{p,n} \delta F^{\omega} + \frac{1}{2}\omega(I_{\rm TOT} + \sum_{p,n} \delta I) \, . \tag{2}$$

The angular velocity ω is tuned to obtain the desired spin given by

$$I_{\rm TOT} = \Im_{\rm rig}\omega + \delta I \, . \tag{3}$$

The liquid-drop energy ($E_{\rm LDM}$) is calculated by summing up the Coulomb and surface energies corresponding to a triaxially deformed shape defined by the deformation parameters β and γ. The rigid-body moment of inertia ($\Im_{\rm rig}$) is calculated with surface diffuseness correction [7]. δF and δI are the shell corrections corresponding to free energy and spin, respectively. To calculate the shell corrections, we use the triaxially deformed Nilsson model together with Strutinsky's prescription. The single-particle energies (e_i^{ω}) and spin projections (m_i) are obtained by diagonalizing the triaxial Nilsson Hamiltonian in a cylindrical representation up to the first twelve major shells. At finite temperatures the free energy in the rotating frame is given by

$$F^{\omega} = \sum_{i=1}^{\infty} e_i^{\omega} n_i - T \sum_{i=1}^{\infty} s_i \, , \tag{4}$$

where s_i are the single-particle entropies and n_i are the occupation numbers which follow the Fermi-Dirac distribution given by

$$n_i = \frac{1}{1 + \exp\left(\frac{e_i^{\omega} - \lambda}{T}\right)} \, . \tag{5}$$

The chemical potential λ is obtained using the constraint $\sum_{i=1}^{\infty} n_i = N$, where N is the total number of particles. The total entropy $S = \sum_{i=1}^{\infty} s_i$ can be represented in terms of occupation numbers as

$$S = -\sum_{i=1}^{\infty} \left[n_i \ln n_i - (1 - n_i) \ln(1 - n_i) \right] \, . \tag{6}$$

The details of the shell correction method at finite T can be found in refs. [7,20]. Here we outline the method illustratively and discuss the estimation of the critical temperature at which shell corrections vanish. The shell correction is given in terms of the single-particle level density as [7,21]

$$\delta F^{\omega} = F^{\omega} - \widetilde{F}^{\omega} = \int_{-\infty}^{\lambda} e \, g(e) \, {\rm d}e - \int_{-\infty}^{\tilde{\lambda}} e \, \widetilde{g}(e) \, {\rm d}e \, , \tag{7}$$

where $g(e) = \frac{{\rm d}\mathcal{N}(e)}{{\rm d}e}$ is the single-particle level density and $\mathcal{N}(e)$ is the total number of particles that can be accommodated by the energy levels with their energy $\leq e$. λ and $\widetilde{\lambda}$ are the chemical potentials corresponding to the discrete and smooth single-particle distributions, respectively. λ and $\widetilde{\lambda}$ can be calculated using the constrains $\mathcal{N}(\lambda) = N$ and $\widetilde{\mathcal{N}}(\widetilde{\lambda}) = N$, respectively. We can also write

$$g(e) = \left. \frac{{\rm d}\mathcal{N}(\lambda)}{{\rm d}\lambda} \right|_{\lambda = e} = \sum_{i=1}^{\infty} \left. \frac{{\rm d}n_i(e_i^{\omega}, \lambda)}{{\rm d}\lambda} \right|_{\lambda = e} \, . \tag{8}$$

From eqs. (5) and (8), we can write the temperature-dependent single-particle level density as

$$g(e) = \sum_{i=1}^{\infty} \frac{1}{4T \cosh^2[(e^{\omega} - e_i)/2T]} \, . \tag{9}$$

From the above relation, it is clear that with the inclusion of temperature the effective energy spectrum is no longer

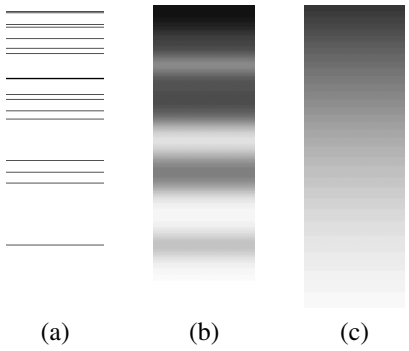

Fig. 1. (a) A typical single-particle energy spectrum. (b) Simulation of the thermal effect on the smoothing of the single-particle spectrum (a) at a temperature of 0.5 MeV. (c) Simulation of Strutinsky smoothing of the single-particle spectrum (a). Now the shell correction comes from the difference between (b) and (c) which will always be less than that between (a) and (c). At higher temperatures, (b) and (c) will be similar leading to the disappearance of shell correction. (In cases (b) and (c) the level densities (9) and (12) are plotted with white representing zero and full black representing values ≥ 1 MeV^{-1}. 254 shades of grey are used to represent intermediate values.)

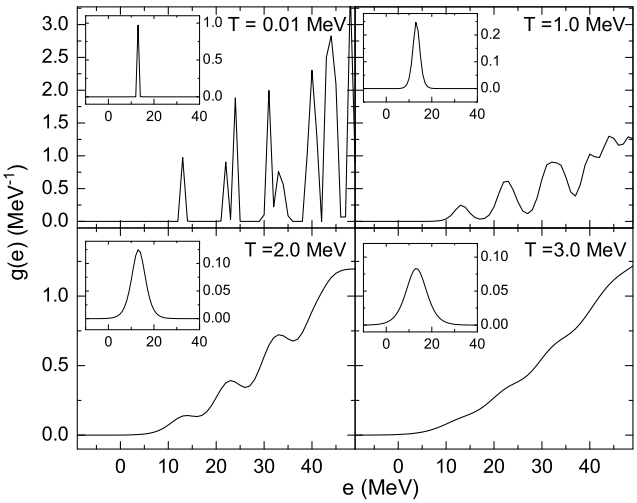

Fig. 2. Temperature-dependent single-particle level densities at different temperatures. The curves in the insets are the first component of $g(e)$ (9). It is evident that the rise in temperature leads to an increase in the width of the components and hence leads to a smooth energy spectrum.

discrete as we allow the level density to vary smoothly with its peaks at discrete levels corresponding to zero temperature. Hence, for hot nuclei the effective single-particle spectrum can be thought as a quasi-continuum whose smoothness increases with temperature. This smoothing of energy levels due to temperature is illustrated in fig. 1b. It has to be noted that the direct effect of temperature in nuclei is the modification of occupation numbers of levels which are still discrete. This, in turn, alters the free energy (4). The alternate view-point of considering the smearing of levels, is useful to understand the role of temperature on shell corrections as explained below.

The natural way of applying Strutinsky averaging to the level density is to convolute $g(e)$ with the averaging function

$$\widetilde{g}(e) = \frac{1}{\gamma_s} \int_{-\infty}^{\infty} \widetilde{f}\left(\frac{e-e'}{\gamma_s}\right) g(e')\, \mathrm{d}e' \,. \qquad (10)$$

We use the averaging function

$$\widetilde{f}(x) = \frac{1}{\sqrt{\pi}} \exp(-x^2) \sum_{m=0}^{p} C_m H_m(x) \,, \qquad (11)$$

where $C_m = (-1)^{m/2}/(2^m(m/2)!)$ if m is even and $C_m = 0$ if m is odd; $x = (e - e_i^{\omega})/\gamma_s$, γ_s is the smearing parameter satisfying the plateau condition $\mathrm{d}\widetilde{F}/\mathrm{d}\gamma_s = 0$; p is the order of smearing and $H_m(x)$ are the Hermite polynomials. When $T = 0$, $g(e')$ is a delta function and we get

$$\widetilde{g}(e) = \sum_{i=1}^{\infty} \widetilde{f}(x) \,. \qquad (12)$$

The above relation can be treated as a representative of a Strutinsky smoothed spectrum as illustrated in fig. 1c. At $T = 0$, we can consider the shell correction energy (7) to be the difference between the energies calculated using, the discrete spectrum (fig. 1a) and the Strutinsky smoothed spectrum (fig. 1c). At finite temperature one has to consider the difference between the temperature smoothed spectrum (fig. 1b) instead of the discrete spectrum (fig. 1a).

Increasing temperature will result in the increase of the width of the function (9) and subsequently will make the level density vary smoothly with respect to the single-particle energy. This situation is well explained by fig. 2, in which the temperature-dependent single-particle level density (9) is plotted as a function of single-particle energy. It is clearly seen in the figure that around $T = 3$ MeV the level density ceases to fluctuate. This form of $g(e)$ at high temperature is very similar to the Strutinsky smoothing function $\widetilde{f}(x)$. In this case, the Strutinsky smoothed spectrum and the effective single-particle spectrum are much similar and hence there is no difference between the two terms in eq. (7). This illustrates the vanishing of the shell correction at high temperatures.

Function (9) is very similar to a Gaussian and we have our Strutinsky smeared single-particle level density as a Gaussian with curvature correction. The relation between the two smoothing quantities could be derived as [22]

$$T \approx 0.472\, \gamma_s \,. \qquad (13)$$

If we have γ_s in the order of the inter-shell spacing ($\hbar\omega$), the above relation suggests that temperatures above half of the inter-shell spacing will wash out shell corrections. The critical temperatures obtained using expression (13) are given in fig. 3. It is evident from the figure that the critical temperature is high for lower-mass nuclei and strongly depend on the smearing parameter γ_s.

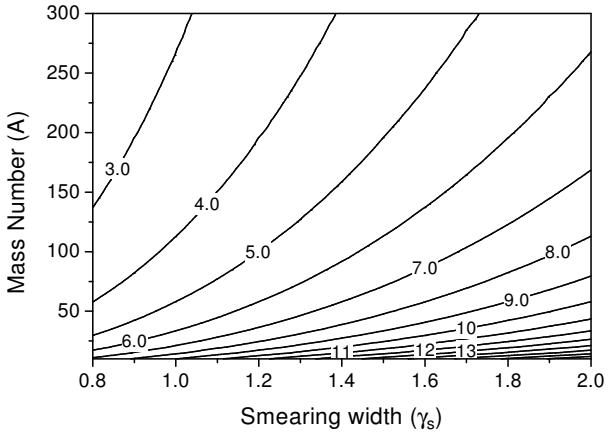

Fig. 3. Upper limits for critical temperatures (in MeV) as a function of mass number and smearing width (in units of oscillator frequency $\hbar\omega_0$).

Substituting eq. (10) in the expression for $\widetilde{F}$ in eq. (7), and using eq. (4), we have [20,21]

$$\widetilde{F}^{\omega} = \sum_i e_i^{\omega}\widetilde{n}_i - T\sum_i \widetilde{s}_i + \gamma_s \int_{-\infty}^{\infty} \widetilde{f}(x)x \sum_i n_i(x)\mathrm{d}x \,, \tag{14}$$

where

$$\widetilde{n}_i = \int_{-\infty}^{\infty} \widetilde{f}(x)\; n_i(x)\; \mathrm{d}x \,, \tag{15}$$

$$\widetilde{s}_i = \int_{-\infty}^{\infty} \widetilde{f}(x)\; s_i(x)\; \mathrm{d}x \,. \tag{16}$$

The integrals appearing in eq. (14) are evaluated numerically using the Hermite-Gauss quadrature. The plateau conditions are observed to be well satisfied with the third term on the right-hand side of eq. (14). The plateaus obtained for the proton shells in ^{208}Pb at different temperatures are shown in fig. 4. We observe that the plateau is clearer for the values of $\gamma_s = 1.6$ and $p = 6$ and we found this to be similar also for neutron shells.

For the spin distribution, the Strutinsky smoothed spin can be derived in a similar way leading to the expression $\widetilde{I} = \sum_{i=1}^{\infty} m_i\widetilde{n}_i$ and hence the shell correction for spin is

$$\delta I = \sum_{i=1}^{\infty} m_i n_i - \sum_{i=1}^{\infty} m_i\widetilde{n}_i \,. \tag{17}$$

2.2 Macroscopic method for GDR

The nuclear shapes are related to the GDR observables using a model [7,23] comprising an anisotropic harmonic-oscillator potential with separable dipole-dipole interaction. In this formalism the GDR frequencies in the laboratory frame are obtained as

$$\widetilde{\omega}_z = (1+\eta)^{1/2}\omega_z \,, \tag{18}$$

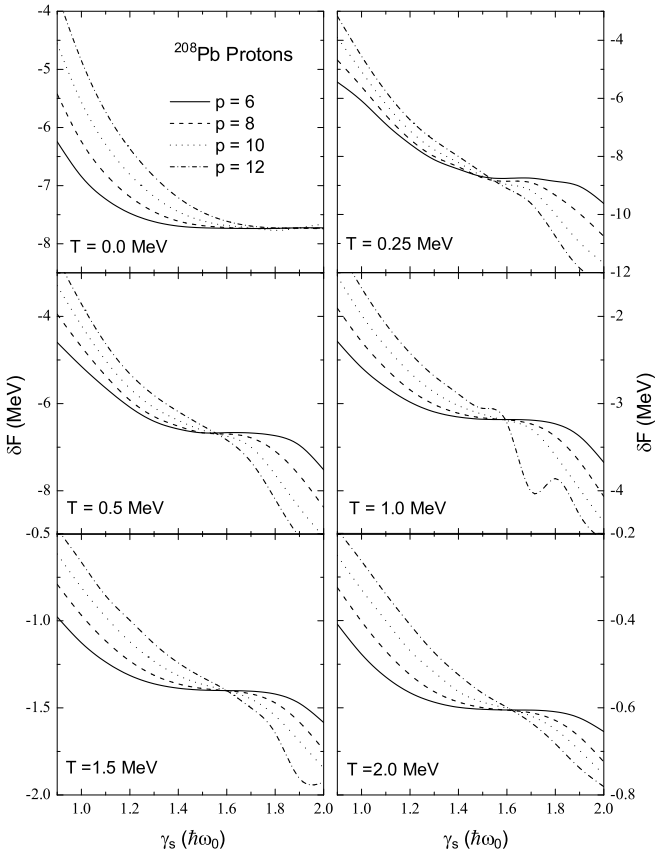

Fig. 4. Shell correction energy as a function of the smearing parameter in the case on ^{208}Pb proton shells at different temperatures. The smearing parameter γ_s is given in units of oscillator level spacing $\hbar\omega_0$.

$$\widetilde{\omega}_2 \mp \Omega = \Bigg\{(1+\eta)\frac{\omega_y^2+\omega_x^2}{2} + \Omega^2 + \frac{1}{2}\Big[(1+\eta)^2(\omega_y^2-\omega_x^2)^2 + 8\Omega^2(1+\eta)(\omega_y^2+\omega_x^2)\Big]^{\frac{1}{2}}\Bigg\}^{\frac{1}{2}} \mp \Omega \,, \tag{19}$$

$$\widetilde{\omega}_3 \mp \Omega = \Bigg\{(1+\eta)\frac{\omega_y^2+\omega_x^2}{2} + \Omega^2 - \frac{1}{2}\Big[(1+\eta)^2(\omega_y^2-\omega_x^2)^2 + 8\Omega^2(1+\eta)(\omega_y^2+\omega_x^2)\Big]^{\frac{1}{2}}\Bigg\}^{\frac{1}{2}} \mp \Omega \,, \tag{20}$$

where Ω is the cranking frequency, ω_x, ω_y, ω_z are the oscillator frequencies derived from the deformation of the nucleus and η is a parameter that characterizes the isovector component of the neutron and proton average field. The GDR cross-sections are constructed as a sum of Lorentzians given by

$$\sigma(E_\gamma) = \sum_i \frac{\sigma_{mi}}{1+\left(E_\gamma^2 - E_{mi}^2\right)^2/E_\gamma^2\Gamma_i^2} \,, \tag{21}$$

where the Lorentz parameters E_m, σ_m and Γ are the resonance energy, peak cross-section and full width at half maximum, respectively. Here i represents the number of components of the GDR and is determined from the shape of the nucleus [23,24]. Γ_i is assumed to depend on the centroid energy through the relation [25]

$$\Gamma_i \approx 0.026 E_i^{1.9} \ . \tag{22}$$

The peak cross-section σ_m is given by

$$\sigma_m = 60 \frac{2}{\pi} \frac{NZ}{A} \frac{1}{\Gamma} \ 0.86(1+\alpha) \ . \tag{23}$$

The parameter α which takes care of the sum rule is fixed at 0.3 for all the nuclei. In most of the cases we normalize the peak with the experimental data and hence the choice of α has less effect on the results. The other parameter η varies with the nucleus so that the ground-state GDR centroid energy is reproduced. The choice for ^{147}Eu is $\eta = 2.8$, for Er isotopes is $\eta = 3.0$ and for ^{179}Au it is $\eta = 3.4$.

2.3 Shape fluctuations

The relation between nuclear shape and GDR cross-section is not straightforward especially in hot nuclei where large-amplitude thermal fluctuations of the nuclear shape play an important role [26]. Hence, for a meaningful comparison of experimental and theoretical values, the thermal shape fluctuations should be taken care of properly. For hot and rotating nuclei there can be fluctuations in the orientation of the nuclear symmetry axis with respect to the rotation axis. The general expression for the expectation value of an observable $\mathcal{O}$ incorporating both thermal and orientation fluctuations is given by [5,27]

$$\bar{\mathcal{O}} = \langle \mathcal{O} \rangle_{\beta,\gamma,\Omega} = \frac{\int \mathcal{D}[\alpha] e^{-F(T,I;\beta,\gamma,\Omega)/T} (\hat{\omega} \cdot \mathcal{I} \cdot \hat{\omega})^{-3/2} \mathcal{O}}{\int \mathcal{D}[\alpha] e^{-F(T,I;\beta,\gamma,\Omega)/T} (\hat{\omega} \cdot \mathcal{I} \cdot \hat{\omega})^{-3/2}} \ , \tag{24}$$

where $\Omega = (\phi, \theta, \psi)$ are the Euler angles specifying the intrinsic orientation of the system, $\hat{\omega} \cdot \mathcal{I} \cdot \hat{\omega} = I_{x'x'} \cos^2\phi \ \sin^2\theta + I_{y'y'} \sin^2\phi \ \sin^2\theta + I_{z'z'} \cos^2\theta$ is the moment of inertia about the rotation axis $\hat{\omega}$ given in terms of the principal moments of inertia $I_{x'x'}$, $I_{y'y'}$, $I_{z'z'}$, and the volume element $\mathcal{D}[\alpha] = \beta^4 |\sin 3\gamma| \, \mathrm{d}\beta \, \mathrm{d}\gamma \, \sin\theta \, \mathrm{d}\theta \, \mathrm{d}\phi$.

In a parametrization based on the Landau theory of phase transitions, developed by Alhassid *et al.* [17,26], the free energy is expanded in terms of certain temperature-dependent constants which are to be extracted by fitting with the free-energy calculations at fixed temperatures from the NS method. Moreover, once the fits involving free energy and moment of inertia are made for the non-rotating case, the calculations can be extended to higher spins using the relation [5]

$$F(T, I; \beta, \gamma, \Omega) = F(T, \omega = 0; \beta, \gamma) + \frac{(I+1/2)^2}{2 \ \hat{\omega} \cdot \mathcal{I} \cdot \hat{\omega}} \ . \tag{25}$$

Hence this theory offers an economic parameterization to study the hot rotating nuclei. While performing high-spin calculations using the above relation, the shell corrections evaluated only at $\omega = 0$ have to be used for all spins. This is not desirable as the single-particle levels swiftly change positions with increasing spin, resulting in a totally different shell structure. We have employed Landau theory in its extended form as given in refs. [7,17] and for the fitting of Landau constants we use the least-squares method.

Thermal shape fluctuation calculations without free-energy parameterizations and consequent fitting are also feasible [7,18,28] by computing the free energies and the observables "exactly" at the integration (mesh) points during numerical integration. In this work we have performed such calculations, however, neglecting the orientation fluctuations. The role of orientation fluctuations is negligible while calculating the scalar observables [7,28, 29] such as the GDR cross-section and width. The GDR observables and free energy are given by the cranking model at a fixed angular frequency (ω). The calculations at fixed spin are performed by adjusting ω to give the desired spin. If this is done independently for each quadrupole deformation, one is led to use an effective volume element in eq. (24) as shown in ref. [29]. This derivation, starting from the partition function at fixed ω, assumes the free energy to have quadratic dependence on ω. In Landau theory the high-spin calculations are done using eq. (25) which satisfies the exact quadratic dependence of free energy on ω. Here we discuss the consequences as the free energy now takes the form of eq. (1). The partition function at fixed angular momentum I is obtained as [29]

$$Z_I(T) = \frac{2I+1}{2\pi i T^2} \int \mathcal{D}[\alpha] \left[\int_{-i\infty}^{i\infty} \mathrm{d}\omega \ \omega \ e^{-[\omega(I+1/2)+F^{\omega}]/T} \right] . \tag{26}$$

The exponent in the above integral can be taken as $-F_{\mathrm{TOT}}/T$ in our case. Letting $\hat{\omega} \cdot \mathcal{I} \cdot \hat{\omega} = \Im_{z'z'} = \Im_{\mathrm{TOT}} = \Im_{\mathrm{rig}} + \delta\Im$ and following the definitions given in ref. [19], we have

$$\mathrm{d}\left[e^{-F_{\mathrm{TOT}}/T}\right] = \Im_{\mathrm{TOT}} \ \omega \ e^{-F_{\mathrm{TOT}}/T} \ \mathrm{d}\omega \ .$$

In the limit $\mathrm{d}\Im_{\mathrm{TOT}}/\mathrm{d}\omega \to 0$, the integration over ω in eq. (26) is analytically solvable leading to an expression having exactly the same form as eq. (24) with $\hat{\omega} \cdot \mathcal{I} \cdot \hat{\omega}$ replaced by $\Im_{\mathrm{TOT}}$. The shell corrections to moment of inertia are significant for spherical shapes which are however suppressed by the term β^4 in $\mathcal{D}[\alpha]$ and for $\beta \geq 0.1$ we have $\Im_{\mathrm{TOT}} \approx \Im_{\mathrm{rig}}$. At high spins also the limiting condition is very much valid as the well-deformed shapes are more favoured. Moreover, the factor arising due to the effective volume element ($\Im_{\mathrm{TOT}}^{-3/2}$) has not much role to play in the practical calculations as shown in ref. [18]. Hence the inclusion of this factor while projecting the fixed angular momentum is not mandatory and has been neglected in some similar calculations [28].

3 Results and discussions

In the present work we have studied few selected nuclei in the mass $140 < A < 180$ region. First we investigate nuclei

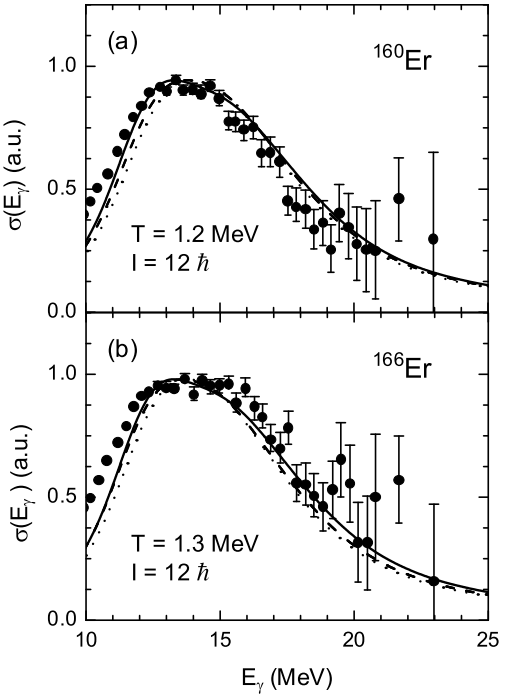

Fig. 5. GDR cross-sections for the nuclei ^{160}Er and ^{166}Er in comparison with experimental data [30] (solid circles). The results from CNSM, Landau, and LDM methods are represented by solid, dashed and dotted curves, respectively.

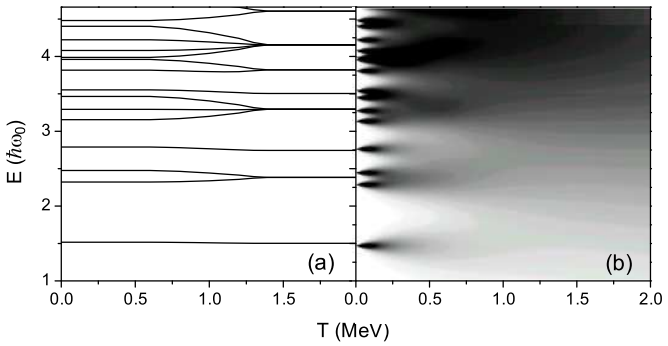

Fig. 6. Simulation of the effect of temperature on the single-particle energy spectrum. The shading in the right panel is done in a similar way as in fig. 1b. As the temperature increases, the discrete single-particle spectrum starts diffusing to a continuum and hence leading to a classical description finally resulting in a spherical shape. This inference could not be obtained at the first sight of the left panel.

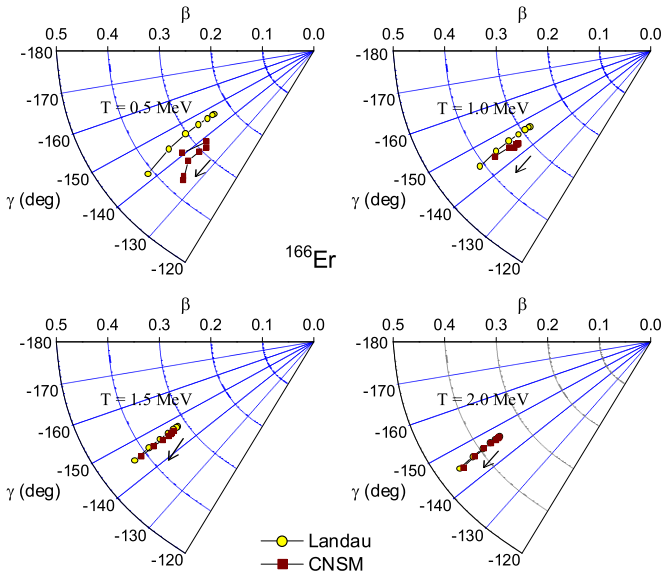

Fig. 7. (Colour online) Hodographs depicting shape transitions in ^{166}Er as a function of spin and temperature. The arrows represent increasing spin which varies from $0\hbar$ to $60\hbar$ in units of $10\hbar$.

with strong deformation in the ground state as we could see the effect of shape transitions as a function of spin and temperature. The calculations are performed with 1) the liquid-drop model (LDM) free energies and Landau theory, 2) NS free energies and Landau theory and 3) cranked NS (CNSM) free energies with the exact treatment of fluctuations.

As representative cases, we study ^{160,166}Er for which experimental data are available. The calculated GDR cross-sections for ^{160,166}Er along with the experimentally observed cross-sections are presented in fig. 5. Calculated results are those obtained using the exact method as well as the Landau theory. From this figure, it is clear that there is no significant difference between the results of exact and Landau calculations. This is because of the weak nature of shell effects in ^{160,166}Er at the measured temperatures. A detailed discussion on the interpretation of this data as well as more general discussions on shape transition in these nuclei can be found in ref. [26]. However, all those arguments are based on calculations at fixed rotational frequency. Here, following a concise interpretation of results, we discuss the shape transitions at low T.

Both the nuclei have a well-deformed prolate shape $\beta = 0.37$; $\gamma = -120°$ for ^{160}Er and $\beta = 0.41$; $\gamma = -120°$ for ^{166}Er at the ground state. At $T = 1.2$ MeV and $I = 12\hbar$, the most probable shape is primarily influenced by the temperature as a consequence of the weakening of shell effects. This situation is illustrated in fig. 6. Due to increase of temperature, the single-particle levels start diffusing, leading to a continuum in which the nucleus behaves classically. On the other hand, the spin induces a shape transition towards a non-collective oblate shape via the spherical shape, even in a rotating liquid drop. Hence, both the temperature and spin drive these nuclei towards a spherical shape. However, the experimental data is well explained by a two-Lorentzian fit showing a finite deformation. This splitting (or broadening) of the GDR line shape could be understood to be due to thermal fluctuations, which allows the non-equilibrium shapes to contribute. In our calculations we find that the averaged deformation parameters are $\overline{\beta} = 0.33$, $\overline{\gamma} = -144.95$ for ^{160}Er and $\overline{\beta} = 0.34$, $\overline{\gamma} = -144.60$ for ^{166}Er.

Even though the experimental data is well understood in terms of shape fluctuations, the data could not directly represent the shape transitions happening in these nuclei.

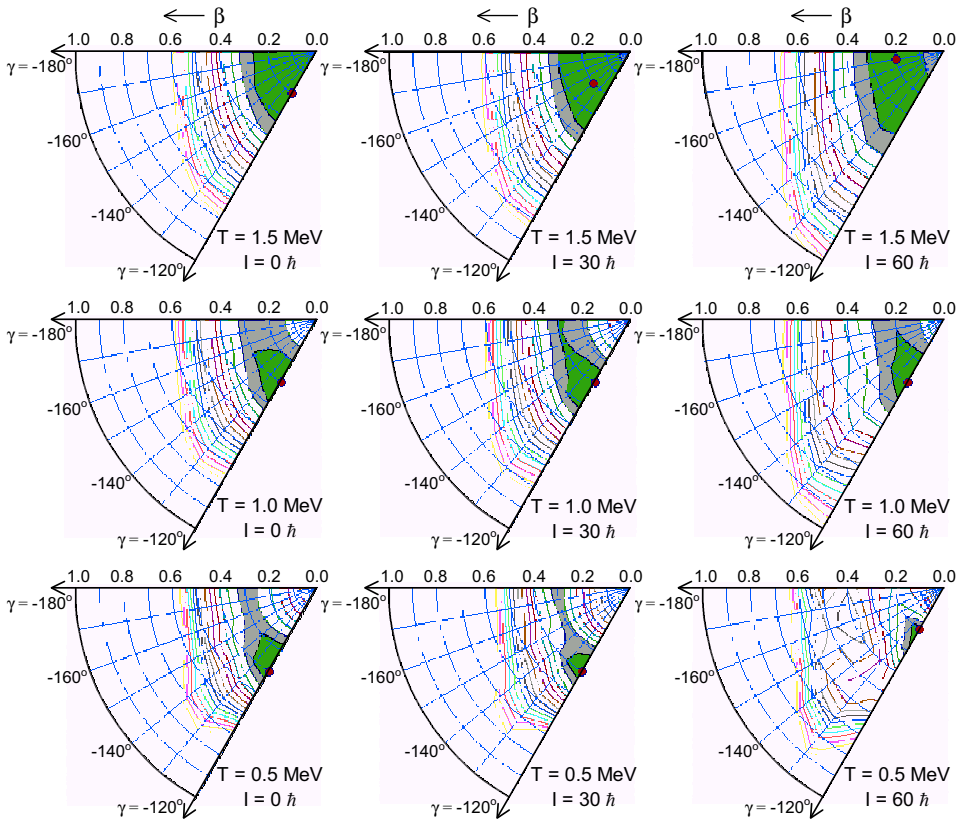

Fig. 8. (Colour online) Potential energy surfaces of the nucleus ^{166}Er at different spins and temperatures. The contour line spacing is 1 MeV. The equilibrium shape is represented by a filled circle and the first two minima are shaded.

The GDR cross-sections could not be easily related to the equilibrium shapes [26] as was done in the ground states. The correlations between the shape and GDR observables are well established [15] to be prominent in spite of the thermal fluctuations. For example, a comparison between the behaviour of $\Gamma_{\rm GDR}$ with spin in the nuclei ^{106,110}Sn and ^{176}W clearly suggests that the shape transitions are well represented by the $\Gamma_{\rm GDR}$ [15]. A very direct relation between the averaged shapes and $\Gamma_{\rm GDR}$ has been recently derived [9]. However, it has to be noted that the GDR could probe shape transitions only if the change in $\bar{\beta}$ is noticeable or rather swift. This swift change in $\bar{\beta}$ in many cases is well suppressed by the fluctuations. Here we show that the use of free-energy parametrizations as well could suppress the sharp changes in $\bar{\beta}$. In fig. 7 we have depicted in hodographs the variation of the averaged shape obtained from the CNSM and Landau calculations. At $T = 0.5$ MeV, $I = 0\hbar$, the exact calculations suggest that the $\bar{\beta}$ is close to its ground-state value. At $I = 10\hbar$, due to the centrifugal effects there is a quenching in the prolate deformation. At higher spins, contributions from high deformations lead to the increase in $\bar{\beta}$. These sharp changes in the averaged shapes are totally missing in the Landau results. Moreover, the trajectory of $(\bar{\beta}, \bar{\gamma})$ as a function of spin is very different from the exact calculations. As suggested in our previous work [18], this discrepancy at low temperature is inherent in the Landau prametrization. At higher temperatures we see that the Landau calculations

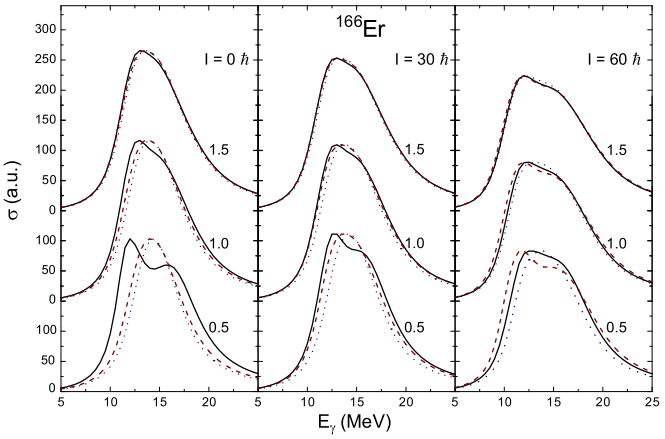

Fig. 9. (Colour online) GDR cross-sections for the nucleus ^{166}Er at different spins and temperatures. The solid, dashed and dotted lines represent results of CNSM, Landau and LDM calculations, respectively. The numbers given to the right of the GDR curves are the corresponding temperatures given in MeV.

do well on a par with exact calculations. Also we see that due to strong fluctuations at higher T, the variation in $(\bar{\beta}, \bar{\gamma})$ is much less.

In fig. 8 we present the potential energy surfaces (PES) of ^{166}Er at different T and I. At $T = 0.5$ MeV we see that the shell effects are stronger keeping intact the well-deformed prolate shape. At $T = 1.0$ MeV, we observe

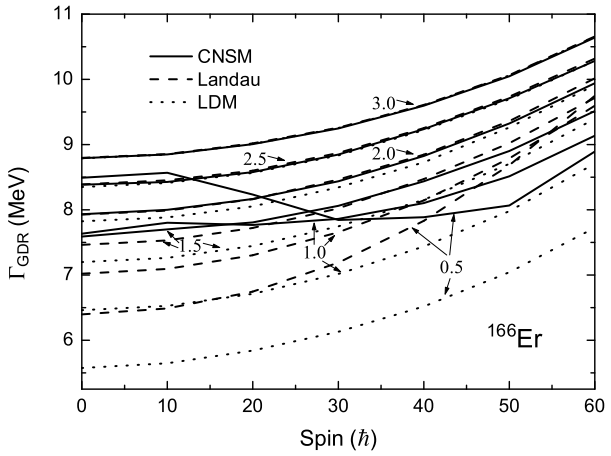

Fig. 10. GDR width for the nucleus ^{166}Er as a function of spin at different temperatures. The numbers near the curves are the corresponding temperatures given in MeV.

a spread in the minimum due to the weakening of shell effects and at $T = 1.5$ MeV the shell effects almost lose their sting as we see a PES resembling a LDM picture. It is instructive to see how well these shape effects are reflected in GDR cross-sections. The results of our GDR cross-section calculations are shown in fig. 9. The shape transitions at $T = 0.5$ MeV are well reflected in the GDR curves. At $T = 0.5$ MeV, $I = 0\hbar$, the GDR curve is well split. As previously discussed, this splitting can arise from two cases *viz*, a) the well-deformed equilibrium shape, b) the dominance of thermal fluctuations. A comparison of the CNSM results with Landau and LDM ones suggests the ruling out of the latter case. If it is due to fluctuations alone, then the Landau and LDM results also should have shown the broadening. At $T = 0.5$ MeV, $I = 60\hbar$, the Landau results suggest a broader curve. This also could be understood due to the difference in the $\bar{\beta}$ values (see fig. 7). At $T = 1.0$ MeV the discrepancy between different methods is marginal which is washed out at $T = 1.5$ MeV.

The calculated $\Gamma_{\rm GDR}$ at different T are presented in fig. 10 as a function of spin. At $T = 0.5$ MeV, the difference in $\Gamma_{\rm GDR}$ values obtained from Landau and CNSM calculations are of the order up to 2 MeV in few cases. The spin-dependence at low T could not be reproduced even qualitatively by the Landau calculations. At $T = 1.0$ MeV, the difference goes up to ~ 0.6 MeV along with the discrepancy in spin-dependence. At $T = 2.0$ MeV, the Landau results go well with exact calculations and at $T = 2.5$ MeV all the results reach the LDM values. Hence, there are interesting shape transitions as a function of spin in ^{166}Er at $T = 0.5$ MeV, which are well reflected in GDR observables. Employing free-energy parameterizations for these cases predicts no significant change in the GDR observables.

Recently the GDR cross-sections of ^{164}Er were measured within a sharp angular-momentum window [31]. The GDR line shapes were reported at spins $I \sim 26\hbar$ and $I \sim 54\hbar$. However, the corresponding temperatures were not reported. We have calculated the GDR cross-sections

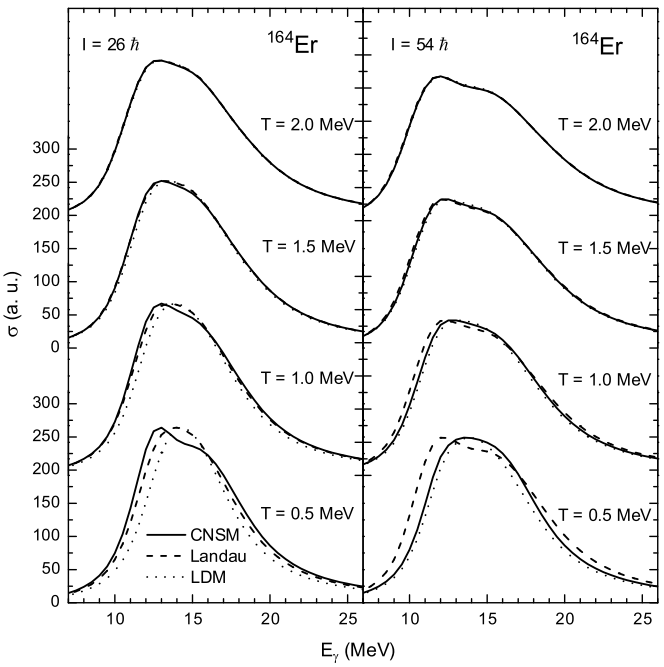

Fig. 11. Temperature dependence of GDR cross-sections for the nucleus ^{164}Er at $I = 26\hbar$ and $I = 54\hbar$.

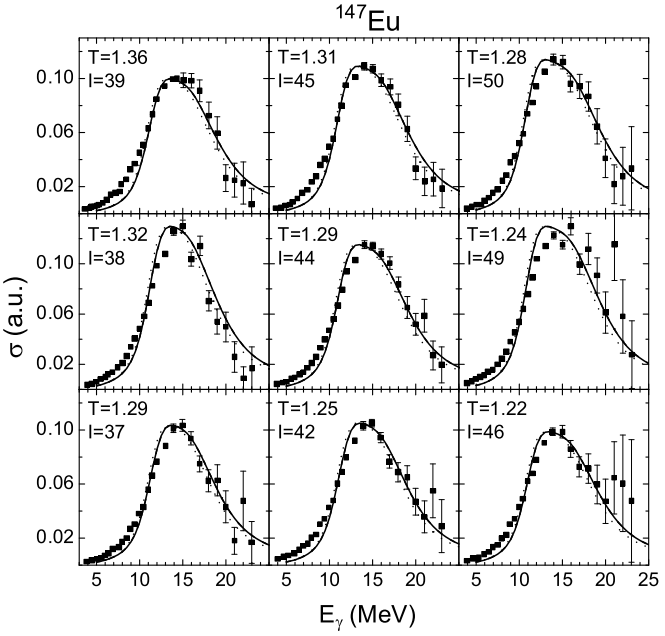

Fig. 12. GDR cross-sections for the nucleus ^{147}Eu in comparison with experimental data [32]. The results from CNSM, Landau, and LDM methods are represented by solid, dashed and dotted curves, respectively.

of ^{164}Er at different temperatures with the spins fixed at $26\hbar$ and $54\hbar$. The results of our calculations are shown in fig. 11. As expected, the results are much similar to those of ^{166}Er. Deviations in Landau results from CNSM ones are noticeable only at $T = 0.5$ MeV and at $T = 1.0$ MeV with the order of difference in $\Gamma_{\rm GDR}$ being 1 MeV and 0.5 MeV, respectively. In both cases the $\Gamma_{\rm GDR}$ by Landau

calculations are lower at $I = 26\hbar$ and are higher at $I = 54\hbar$. Hence, the trend in spin-dependence of $\Gamma_{\rm GDR}$ could not be reproduced by the Landau calculations. This is due to the fact that the spin-dependence of the shell correction energy is not taken care of by the Landau parametrization. Our study suggests that for an accurate description of the GDR observables at $T \leq 1$ MeV in ^{166}Er we should employ an exact calculation of the fluctuations.

The spin-dependence of GDR observables is measured recently in the case of ^{147}Eu [32]. Observations were done in the spin range $37\hbar$–$50\hbar$ within a narrow temperature range around $T \sim 1.3$ MeV. The measured cross-sections at different T and I are presented in fig. 12 along with our theoretical results. The agreement between theory and experiment turns out to be good, as seen in the figure. Our results are much closer to the theoretical values (not shown here) reported in [32]. Also we see that spin-driven shell effects have no role to play as the CNSM and Landau results are almost the same in these temperatures. In fact the proton and neutron shell corrections are weak and they act against each other. The averaged shapes felt by ^{147}Eu at $T = 1.3$ MeV are plotted in fig. 13a as a function of spin. A gradual increase in the $\bar{\beta}$ could be seen and this leads to the broadening of GDR curves as the spin increases. This feature is well depicted by the GDR curves in fig. 12. In fig. 13b, we present the $\Gamma_{\rm GDR}$ also along with the $\bar{\beta}$. Both the experimental and theoretical values are shown in this figure. Good conformity between these values could be seen in the figure. In the same figure we have included our results calculated also at $T = 0.5$ MeV. In fig. 14, the potential energy surfaces calculated by CNSM are depicted. At $\omega = 0$, the shell corrections are strong (~ 2 MeV for the equilibrium shape which is spherical) resulting in a crisp minimum around the spherical shape. Hence, the $\Gamma_{\rm GDR}$ at $\omega = 0$ is expected to be lower than the LDM predictions similar to the case of ^{208}Pb [7]. As the spin increases, the minimum shifts towards the oblate shape with $\beta \sim 0.1$ up to $30\hbar$. At $40\hbar$ one can see from fig. 14 a jump in the minimum towards $\beta \sim 0.3$. We see in fig. 13a that the change in β is carried over to $\bar{\beta}$ in the CNSM results. The variation in $\bar{\beta}$ is well reflected also in $\Gamma_{\rm GDR}$. Hence these shape transitions do survive thermal fluctuations and could be reflected in GDR observables. However, this is the case with CNSM calculations only. The shape transitions are totally washed out in the Landau calculations. The Landau results are closer to LDM results and hence could not account properly for the shell effects. At low temperatures of the order of 0.5 MeV, we could have better direct correlations between the shapes and the GDR observables only if we adopt CNSM calculations. Recent low-temperature measurements are discussed below.

The low-temperature GDR measurements have been reported for the nuclei ^{120}Sn [10] and ^{179}Au [11]. The GDR width of ^{120}Sn was measured [10] at $T = 1.0$ MeV to be 4 ± 1 MeV. This width was found to be much lower than the predictions of thermal-fluctuation models (~ 7 MeV). In our earlier calculations [7] we found that the shell corrections do not have any role to play in the case of ^{120}Sn. This rules out the proper treatment of shell effects to interpret the low-T data. Very recently, this anomaly could be understood as a consequence of fluctuations in the pairing field [8]. Hence, the low-temperature GDR measurements have proved that the pairing plays a vital role. In the present work, we have not considered the pairing correlations. However, we discuss problems apart from this, *i.e.*, the discrepancy in free-energy parametrizations and the direct correlations between shape transitions and GDR observables. As another supportive case, we discuss here the low-T observations in ^{179}Au [11]. Also in this nucleus, at $T = 0.7$ MeV, the $\Gamma_{\rm GDR}$ was observed to be much less than the thermal-fluctuation model predictions. The observed width is 5.0 ± 0.35 MeV, whereas the LDM with thermal fluctuation predicts ~ 7 MeV. Initially shell effects were attributed for the lowering of $\Gamma_{\rm GDR}$ [11], which we have ruled out in our previous work [18]. Only pairing fluctuations are expected to explain this lowering of $\Gamma_{\rm GDR}$. In fig. 15, we show the calculated GDR cross-sections for ^{179}Au at different temperatures and spin. The overall observations are very much similar to the case of ^{164,166}Er except that this nucleus undergoes a shape transition to a strongly deformed shape around $60\hbar$. All the three methods predict almost the same cross-section at this point, too. At $T = 0.7$ MeV, the difference between $\Gamma_{\rm GDR}$ by exact and other methods comes out to be ~ 0.3 MeV. The reason for this discrepancy is the shell effects, which leads to shape coexistence. In fig. 16, we have plotted the potential energy curves as a function of T. Coexisting oblate and prolate shapes which have much lower energy than the spherical state could be seen at low T. Around $T \sim 1.0$ MeV the nucleus attains a spherical shape. In

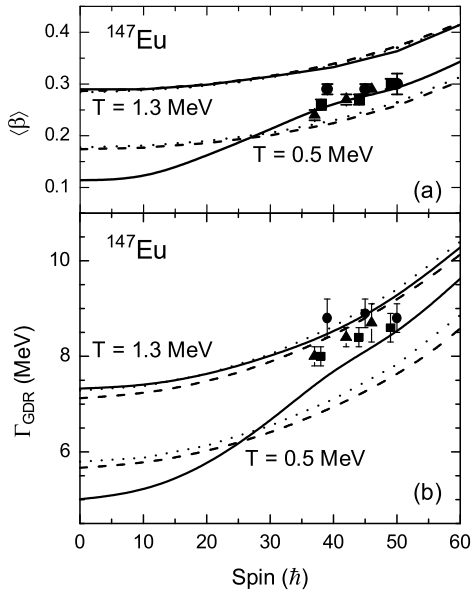

Fig. 13. GDR width and the averaged deformations for the nucleus ^{147}Eu as a function of spin ($I\hbar$) The solid circle, solid square and solid triangle correspond to experimental data [32] at beam energies 170, 165 and 160 MeV, respectively. These energies correspond to temperatures from 1.2 to 1.4 MeV [32]. The results from CNSM, Landau, and LDM methods are represented by solid, dashed and dotted curves, respectively.

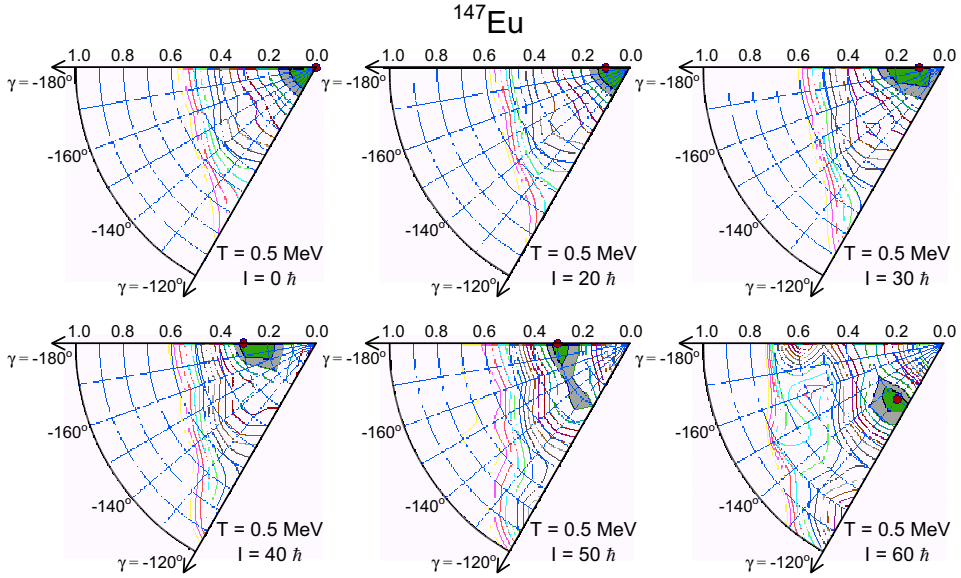

Fig. 14. (Colour online) Potential energy surfaces of the nucleus ^{147}Eu at different spins and at $T = 0.5$ MeV. The contour line spacing is 1 MeV. The equilibrium shape is represented by a filled circle and the first two minima are shaded.

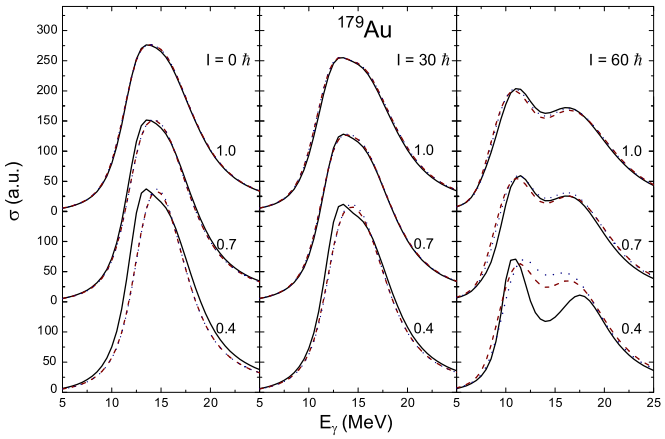

Fig. 15. (Colour online) GDR cross-sections for the nucleus ^{179}Au at different spins and temperatures. The solid, dashed and dotted lines represent results of CNSM, Landau and LDM calculations, respectively. The numbers given to the right of the GDR curves are the corresponding temperatures given in MeV.

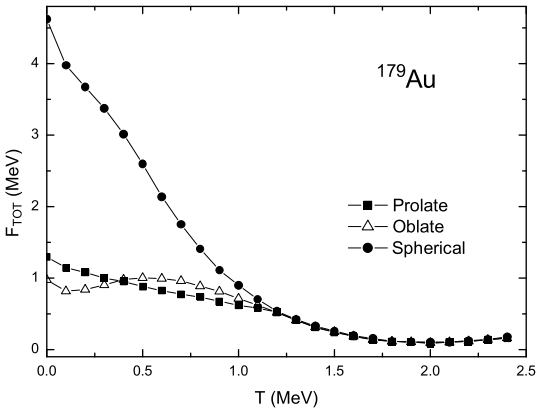

Fig. 16. Potential (free) energy curves for different shapes for the nucleus ^{179}Au as a function of T. At low temperatures, shape coexistence can be seen and at $T \sim 1.0$ MeV the nucleus attains a spherical shape.

fig. 17, we depicted the spin-dependence of $\Gamma_{\rm GDR}$ of ^{179}Au at $T = 0.7$ MeV. The exact calculations suggest weak spin-dependence and the trend of the curves by exact and other calculations are significantly different.

4 Conclusions

We have presented our macroscopic approach towards GDR with the details concerning the shell correction procedure at high spin and temperature. Thermal shape fluctuations are treated with and without free-energy parameterization. Shape transitions at low temperature in ^{160,164,166}Er are discussed along with their effects in GDR observables. Our low-T calculations predict that the discrepancies in using free-energy parameterizations could alter the GDR width up to 2 MeV in certain cases. Recently, observed GDR cross-sections and widths of ^{147}Eu at different temperature and spin could be well understood by our calculations. We have shown that if the fluctuations are treated properly, then, in spite of thermal fluctuations, GDR observables could very well reflect the shape transitions at low temperature. Calculations using free-energy parameterizations predict that these transitions could not effect significant changes in GDR observables due to thermal fluctuations. Our calculations rule out the possibility that at low T, within a thermal-fluctuation model, a proper treatment of shell corrections could explain the quenching in the GDR width. Any complete description of nuclei at low T should comprise pairing correlations. Work is in progress to incorporate them in our framework. Besides neglecting the role of pairing correlations, our low-T

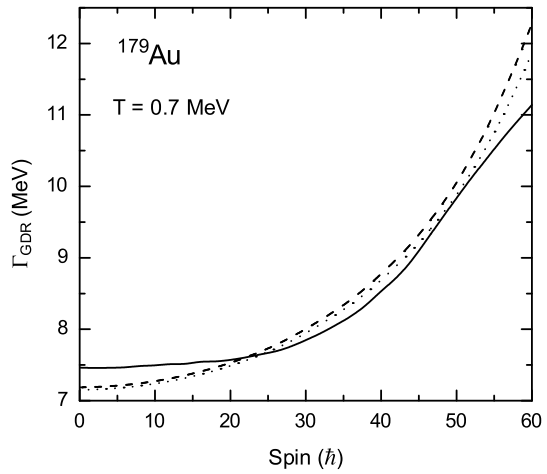

Fig. 17. GDR width for the nucleus ^{179}Au as a function of T. The results from CNSM, Landau, and LDM methods are represented by solid, dashed and dotted curves, respectively.

calculations clearly and quantitatively bring out the discrepancies in using free-energy parametrizations and suggest that in spite of thermal fluctuations, GDR could effectively probe the sharp transitions which were predicted to be washed out when free-energy parametrizations are employed.

References

1. K.A. Snover, Annu. Rev. Nucl. Part. Sci. **36**, 545 (1986); J.J. Gaardhøje, Annu. Rev. Nucl. Part. Sci. **42**, 483 (1992).
2. V. Baran, M. Colonna, M. Di Toro, A. Guarnera, V.N. Kondratyev, A. Smerzi, Nucl. Phys. A **599**, 29 (1996).
3. N.D. Dang, K. Tanabe, A. Arima, Phys. Lett. B **445**, 1 (1998); Nucl. Phys. A **645**, 536 (1999).
4. M. Gallardo, M. Diebel, T. Døssing, R.A. Broglia, Nucl. Phys. A **443**, 415 (1985).
5. Y. Alhassid, Nucl. Phys. A **649**, 107c (1999).
6. W.E. Ormand, P.G. Bortignon, R.A. Broglia, Nucl. Phys. A **614**, 217 (1997).
7. P. Arumugam, G. Shanmugam, S.K. Patra, Phys. Rev. C **69**, 054313 (2004).
8. N.D. Dang, A. Arima, Phys. Rev. C **68**, 044303 (2003).
9. D. Kusnezov, W.E. Ormand, Phys. Rev. Lett. **90**, 042501 (2003).
10. P. Heckman *et al.*, Phys. Lett. B **555**, 43 (2003).
11. F. Camera *et al.*, Phys. Lett. B **560**, 155 (2003).
12. A. Bracco, Acta Phys. Pol. B **34**, 2163 (2003).
13. S.K. Rathi, D.R. Chakrabarty, V.M. Datar, S. Kumar, E.T. Mirgule, A. Mitra, V. Nanal, H.H. Oza, Phys. Rev. C **67**, 024603 (2003).
14. M. Thoennessen, Nucl. Phys. A **731**, 131 (2004).
15. A. Bracco *et al.*, Nucl. Phys. A **599**, 83c (1996).
16. S.F. Mughabghab, A.A. Sonzogni, Phys. Rev. C **65**, 044620 (2002).
17. Y. Alhassid, B. Bush, Nucl. Phys. A **549**, 12 (1992).
18. P. Arumugam, A. Ganga Deb, S.K. Patra, Europhys. Lett. **70**, 313 (2005).
19. K. Neergård, V.V. Pashkevich, S. Frauendorf, Nucl. Phys. A **262**, 61 (1976).
20. M. Brack, P. Quentin, Nucl. Phys. A **361**, 35 (1981).
21. G. Shanmugam, P. Arumugam, Pramana J. Phys. **57**, 223 (2001).
22. L.G. Moretto, Phys. Lett. B **38**, 393 (1972).
23. G. Shanmugam, M. Thiagasundaram, Phys. Rev. C **37**, 853 (1988); **39**, 1623 (1989).
24. R.R. Hilton, Z. Phys. A **309**, 233 (1983).
25. P. Carlos, R. Bergere, H. Beil, A. Lepretre, A. Veyssiere, Nucl. Phys. A **219**, 61 (1974).
26. Y. Alhassid, B. Bush, Nucl. Phys. A **509**, 461 (1990).
27. Y. Alhassid, B. Bush, Nucl. Phys. A **531**, 39 (1991).
28. A. Ansari, N.D. Dang, A. Arima, Phys. Rev. C **63**, 024310 (2003).
29. W.E. Ormand, P.G. Bortignon, R.A. Broglia, Nucl. Phys. A **618**, 20 (1997).
30. J.J. Gaardhøje, C. Ellegaard, B. Herskind, S.G. Steadman, Phys. Rev. Lett. **53**, 148 (1984).
31. V. Nanal *et al.*, Nucl. Phys. A **731**, 153 (2004).
32. M. Kmiecik *et al.*, Nucl. Phys. A **674**, 29 (2000).